On the evolution of nanocluster size distribution in a nanocluster aggregation source

Turkin, A. A.; Dutka, M. V.; Pei, Y. T.; Vainchtein, D. I. ; de Hosson, J. Th. M.

Published in:
Journal of Applied Physics

DOI:
10.1063/1.4731221

On the evolution of nanocluster size distribution in a nanocluster aggregation source

A. A. Turkin,[1,2] M. V. Dutka,[1] Y. T. Pei,[1] D. I. Vainshtein,[1] and J. Th. M. De Hosson[1,a)]
[1]*Department of Applied Physics, Materials Innovation Institute M2i and Zernike Institute for Advanced Materials, University of Groningen, Nijenborgh 4, 9747 AG Groningen, The Netherlands*
[2]*National Science Center "Kharkov Institute of Physics & Technology," Akademicheskaya str. 1, UA-61108 Kharkov, Ukraine*

(Received 25 February 2012; accepted 19 May 2012; published online 27 June 2012)

This paper presents a detailed model of cluster formation from a supersaturated atomic vapor in an inert buffer gas. The population balance equations for the cluster size distribution are based on the Smoluchowski coagulation equation and take into account (i) convective diffusion of clusters, (ii) cluster loss to walls of an aggregation chamber, and (iii) formation of fractal-like aggregates. The model predictions are confronted to experimental observations, and they agree with experimental data on Cu particle formation in NC200-UHV nanocluster source. The model can be used as an aid in tuning the experimental parameters for attaining a desired nanoparticle size distribution. © *2012 American Institute of Physics*. [http://dx.doi.org/10.1063/1.4731221]

I. INTRODUCTION

At present nanoparticles and nanoclusters attract great interest in scientific research and industrial applications including microelectronics, optics, catalysis, medicine, biology, etc., owing to their unique size-dependent physical and chemical properties.[1–4] Nanoparticles are produced both by chemical and physical methods.[2] In this paper, we will consider nanocluster production from a supersaturated atomic vapor in a gas aggregation chamber where atomic vapor mixes with a stream of inert gas. Clusters grow in the aggregation chamber until the mixture of gas and clusters is transferred through an aperture into a surrounding vacuum chamber. By changing experimental parameters particle size, morphology and composition can be manipulated to produce materials of desired properties. Nanoparticle growth is affected by several factors, such as the residence time of clusters in the aggregation chamber, the temperature inside the aggregation chamber, and the ratio of the atomic vapor to the inert gas.

A very important property of the aggregation process is the particle size distribution (PSD) that affects the properties of the final product, e.g., a nano-structured material with broad cluster-size dispersion will exhibit a lower overall flow stress than a material with the same average cluster size but with a narrow cluster-size distribution. Consequently, experimental control over the cluster-size distribution is important in designing nano-structured materials. The particle size distributions can largely vary in time. Computer modeling of nanocluster formation and evolution is a well suited method to study and predict effects of operating conditions on PSD. In particular, Monte Carlo simulations[5,6] have provided useful insights on cluster formation kinetics. However, Monte Carlo simulations are limited to rather small number of atoms in clusters because of significant computational limitations. Real length and time scales of experiments are presently out of reach of Monte Carlo simulations.

In this paper, we develop a mean-field description of PSD evolution via cluster coagulation driven by Brownian motion in the aggregation chamber (Sec. II). Aggregation phenomena are quite common in nature, e.g., aerosol physics[7] and particle synthesis in flames.[8,9] Theoretical studies of particle coagulation are frequently based on the assumption of instantaneous and complete coalescence of colliding particles, which results in the formation of spherical particles. In our experiments, we have observed that nanoclusters often form dendritic structures that are called in literature "fractal-like." These agglomerates can be characterized by a fractal dimension[10] $D_f < 3$. The model developed in Sec. II for the spherical nanoclusters is further modified to account for the fractal-like nanoclusters. To this end, we use the concept of an effective collision cross-section of fractal-like cluster,[11,12] which is larger than the collision cross-section of the spherical cluster of the same mass. The fractal dimension is assumed to depend on the number of atoms in clusters. The simulation results are discussed in Sec. III and compared to experimental data in Sec. IV.

II. MODEL

The model presented is confronted to experiments of Cu cluster formation in the NC200-UHV nanocluster source manufactured by Oxford Applied Research. For sake of clarity, in the following, we will refer to the operating conditions and configuration of this equipment. The aggregation chamber is shown schematically in Fig. 1. It is similar to a chemical gas flow reactor. A magnetron sputtering device is used to feed the supersaturated atomic vapor into the aggregation tube from the left. An inert gas, usually argon, is injected into the aggregation tube simultaneously with the atomic vapor of clustering material. Argon flow transports atoms and clusters along the aggregation region towards an aperture.

a)Author to whom correspondence should be addressed. Electronic mail: j.t.m.de.hosson@rug.nl. Tel.: +31-50-363 4898. Fax: +31-50-363 4881.

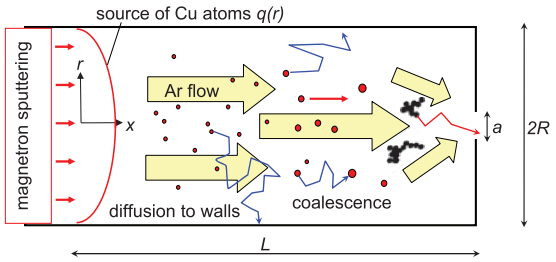

FIG. 1. Schematic illustration of cluster formation from the atomic vapor. At $x=0$, all species are assumed to reach thermal equilibrium through mutual collisions and interactions. Clusters drift along the aggregation tube with the gas drift velocity; they grow in size via collisions with each other which result in coalescence. Because of diffusion, Cu atoms and clusters are lost to wall. At a latter stage, clusters are fractal-like, i.e., clusters are shaped like dendritic aggregates.

Our objective is to find the nanoparticle size distribution as a function of distance along the aggregation tube. This distribution is defined by densities of clusters of all sizes $C_k(x)$, where $k>1$ is the number of atoms in clusters. Rather than go into the detail of producing Cu vapor, we will use a plausible shape of the Cu atom source (Fig. 1). The total flux of Cu atoms from the target was found by measuring mass loss during target sputtering for a given period of time. Typical parameters of the aggregation process are listed in Table I.

The rate of Ar flow Q_{Ar} is related to the mean drift velocity of Ar gas v in the aggregation zone and the gas effusion velocity through the aperture v_{out}

$$Q_{Ar} = \pi R^2 v C_{Ar} = \frac{1}{4}\pi a^2 v_{out} C_{Ar}, \tag{1}$$

where R is the tube radius, a is the diameter of the aperture (Fig. 1), and C_{Ar} is the density of Ar gas. It is known that the gas effusion velocity can be estimated as[13]

$$v_{kin} < v_{out} < v_{hyd}, \tag{2}$$

v_{kin} is the effusion velocity in the kinetic regime when the mean free path of gas atoms is about or larger than the diameter of the aperture

$$v_{kin} = \frac{1}{4}\sqrt{\frac{8k_BT}{\pi m_{Ar}}}, \tag{3}$$

TABLE I. Basic set of parameters used for simulation of cluster formation.

Parameter	Value
Length of aggregation chamber, L (mm)	200
Radius of aggregation chamber, R (mm)	50
Aperture diameter, a (mm)	3
Temperature, T (K)	300
Rate of Ar flow, Q_{Ar}, sccm (s^{-1})	16.8 (7.5×10^{18})
Argon pressure, P_{Ar} (Pa)	40
Total flux of Cu atoms sputtered from the target, Q_{Cu} (s^{-1})	7.1×10^{17}
Sticking coefficient for the dimer formation, η_{11}	$1.8\times10^3 C_{Ar} r_{Ar}^3$
Fractal dimension of large clusters, D_f^{∞}	1.8
Maximum number of atoms in a cluster with $D_f(k)=3$, k_0	1100

where k_B is the Boltzmann's constant, T is the temperature, and m_{Ar} is the atomic mass of Ar. If the aperture diameter is much larger than the mean free path of molecules, the gas outflow is hydrodynamic, i.e.,

$$v_{hyd} = \left(\frac{2}{\gamma+1}\right)^{\frac{\gamma+1}{2(\gamma-1)}}\sqrt{\frac{\gamma k_BT}{m_{Ar}}}, \tag{4}$$

where $\gamma=5/3$ is the adiabatic exponent.

Using the ideal gas law, the upper, and lower bound of Ar pressure P_{Ar} inside the aggregation tube can be estimated. However, in our case, the Ar pressure is measured directly; therefore, the mean drift velocity of Ar gas in the aggregation zone is given by

$$v = \frac{k_BTQ_{Ar}}{\pi P_{Ar}R^2} = 0.099\,\mathrm{m/s}. \tag{5}$$

We note that

$$v \approx 1.1 v_{kin}. \tag{6}$$

We will use this relation later, assuming that the Ar pressure is proportional to the rate of Ar flow Q_{Ar}. The Ar density at the parameters indicated in Table I is $C_{Ar}=9.7\times10^{21}\,\mathrm{m}^{-3}$.

To describe cluster diffusion and collisions among the clusters, we use the gas kinetic theory.[13,14] The mean collision free path λ of argon atoms is about 0.5 mm, namely, it satisfies inequalities $R_k \ll \lambda \ll R$, where R_k is the cluster radius. Under typical conditions precursor atoms and clusters form a dilute gas mixture in argon gas $C_k \ll C_{Ar}$, $k \geq 1$. This means that clusters collide more frequently with Ar atoms; hence, diffusion of each cluster class can be considered separately as diffusion in a binary mixture. For the diffusion coefficient of clusters of size k, we use a formula for rigid spheres of unequal masses[14]

$$D_k = \frac{1}{3}\sqrt{\frac{2}{\pi}}\sqrt{\frac{1}{m_{Ar}}+\frac{1}{k\,m_{Cu}}}\frac{(k_BT)^{3/2}}{P_{Ar}\pi(r_{Ar}+r_{Cu}k^{1/3})^2}, \tag{7}$$

where m_{Cu} is the atomic mass of Cu and $r_{Cu,Ar}$ are the atomic radii of Cu and Ar atoms.

To describe the evolution of PSD, we use a mean-field approach based on the Smoluchowski coagulation equation[15] for the growth of clusters by successive mergers. The model makes the following assumptions about cluster growth:

- Gas of metal atoms is unstable with respect to cluster nucleation and coagulation.
- Two colliding spherical clusters coalesce instantaneously to form a larger cluster, the mass of the resulting particle being the sum of the masses of the colliding particles.
- Except during collisions, the interactions among clusters are negligible.
- No fragmentation of colliding clusters occurs.
- No thermal dissolution of clusters by monomer evaporation from the cluster surface.
- Clusters suspended in Ar gas undergo random walks and drift downstream with the velocity of Ar flow.

The coagulation kinetics is superimposed upon the convective diffusion process. Therefore, the population balance

equation (PBE) describing the formation and evolution of PSD is essentially similar to that used in aerosol science,[7]

$$\frac{\partial C_k(r,x,t)}{\partial t} + div(-D_k \nabla C_k + vC_k) = \frac{1}{2}\sum_{i=1}^{k-1} w_{i,k-i} C_i C_{k-i} - C_k \sum_{i=1}^{\infty} w_{ik} C_i \quad k \geq 2. \tag{8}$$

Equation for the monomer density is given by

$$\frac{\partial C_1(r,x,t)}{\partial t} + div(-D_1 \nabla C_1 + vC_1) = -C_1 \sum_{k=1}^{\infty} w_{1k} C_k. \tag{9}$$

The first term in the right hand side of Eq. (8) is the rate at which clusters of size k are formed by coagulation and the second term is the rate at which clusters are lost by growth to larger sizes. The boundary conditions for Eqs. (8) and (9) correspond to cluster adsorption by the inner walls

$$C_k|_{r=R} = 0, \quad C_k|_{x=L} = 0 \quad k \geq 1; \tag{10}$$

and a steady feed-in of monomers into the aggregation zone

$$(-D\nabla C_1 + vC_1)|_{x=0} = q(r), \tag{11}$$

where a parabolic shape of the source of Cu atoms from the target is assumed

$$q(r) = \frac{2Q_{Cu}}{\pi R^2}\left(1 - \frac{r^2}{R^2}\right), \quad \int_0^R 2\pi r q(r) dr = Q_{Cu}. \tag{12}$$

In the following, we will be interested in PSD variation along the axis of the aggregation tube. To find the solution of Eqs. (8) and (9), we neglect the radial dependence of the gas flow velocity and approximate it by a plug flow with velocity given by Eq. (5). With the constant rate of monomer supply into the aggregation tube, the system reaches a steady state $\partial C_k/\partial t = 0$. Further simplification is achieved by replacing the diffusion operator with multiplication by the constant (see Appendix A),

$$D_k \Delta C_k \Rightarrow -v\mu(D_k) C_k, \quad \mu(D_k) = \frac{v}{2D_k}\left(\sqrt{1 + \left(\frac{2D_k}{vR}\right)^2 {\beta_1}^2} - 1\right). \tag{13}$$

Finally, the set of equations for PSD is reduced to

$$\frac{\partial C_1}{\partial \tau} = -v\mu(D_1) C_1 - C_1 \sum_{i=1}^{\infty} w_{i,1} C_i, \tag{14}$$

$$\frac{\partial C_k}{\partial \tau} = -v\mu(D_k) C_k + \frac{1}{2}\sum_{i=1}^{k-1} w_{i,k-i} C_i C_{k-i} - C_k \sum_{i=1}^{\infty} w_{ik} C_i \quad k \geq 2, \tag{15}$$

$$C_1|_{x=0} = C^0_{axis}, \tag{16}$$

$$C_k|_{x=0} = 0 \quad k \geq 2. \tag{17}$$

Here, we introduced the "stream-time" $\tau = x/v \leq \tau_{max}$, $\tau_{max} = L/v \sim 2$ s is the residence time of Cu clusters in the aggregation tube. The starting value for monomer density C^0_{axis} is estimated from the solution of diffusion equation for monomer without coagulation (see Appendix A).

A. Coagulation kernel

Assuming thermal velocities for all the k-mers, the collision frequency function or the coagulation kernel of spherical clusters is given by[7]

$$w_{ij} = \eta_{ij} (R_i + R_j)^2 \sqrt{\frac{8\pi k_B T}{m_{Cu}}\left(\frac{1}{i} + \frac{1}{j}\right)}, \tag{18}$$

where $R_i = r_{Cu}\sqrt[3]{i}$ is the radius of the cluster containing i atoms. We introduced into Eq. (18) the sticking coefficient η_{ij} because not all collisions result in cluster coalescence. This is especially true for the formation of dimers and small clusters. As early as 1898, Boltzmann postulated that atom-atom recombination involves three body collisions because of energy and momentum conservation.[16] The dimer forms in a two-step process (energy transfer mechanism).[17] Two colliding atoms may form a metastable excited Cu_2^* orbiting complex

$$Cu + Cu \Longleftrightarrow Cu_2^*. \tag{19}$$

The collision complex can be stabilized, if the third atom (Ar or Cu) collides within the lifetime of the complex and carries away the excess internal energy of the dimer. In our case, the third atom is an Ar atom, since $C_{Ar} \gg C_{Cu}$,

$$Cu_2^* + Ar \Rightarrow Cu_2 + Ar^*. \tag{20}$$

Derivation of the sticking coefficient for dimer formation is presented in Appendix B.

While clusters grow, they are heated by the binding energy delivered by aggregating atoms and clusters, i.e., by the latent heat of condensation.[5] The excess energy is dissipated by inelastic collisions with the inert buffer gas. In addition, at low temperatures, the excess energy is spent to atomic rearrangements leading to the spherical shape of small clusters. This means that the sticking coefficient η_{ij} tends to a value close to unity as one of indices (i or j) increases, i.e., all cluster collisions result in coagulation. In the following, we assume that the sticking coefficients $\eta_{ij} = 1$ for $i + j > 4$. To ensure a smooth transition to $\eta_{ij} = 1$, the following values of the sticking coefficients are taken for cluster sizes satisfying inequalities $2 < i + j \leq 4$:

$$\eta_{12} = 10^2 \eta_{11}, \; \eta_{13} = \eta_{22} = 10^4 \eta_{11}. \tag{21}$$

The coefficients given by Eq. (21) are somewhat arbitrary; they are selected to fit our experimental data. However, we have found that essentially the same results for PSD evolution can be obtained with more sophisticated parametrizations. Modeling shows that the PSD evolution is the most sensitive to variation of sticking coefficients for clusters with sizes in the range $2 \leq i + j \leq 4$.

When clusters become sufficiently large, the condensation energy is not enough for complete coalescence or sintering of clusters. If the time of thermal sintering of colliding clusters is longer than the mean time between successive collisions, the aggregates grow dendrite- or fractal-shaped and their morphology can only be characterized at the statistical level by the fractal dimension D_f. This means that the coagulation kernel for spherical clusters, Eq. (18), is no longer valid for large clusters.

In three dimensional, space diffusion-limited cluster aggregation leads to fractal aggregates with a typical value[7,18,19] of $D_f \sim 1.8$. The behavior of fractal-like aggregates, and spherical particles of the same mass is different. The fractal-like structure significantly affects the frequency of collisions and the rate of coagulation. Following Refs. 7, 11, and 12, we will describe collisions between fractal-like particles as collisions of spherical particles each having an effective collision radius. Models for particle coagulation that we found in the literature assume that there is a unique value of the fractal dimension for all aggregates in the ensemble. However, in real coagulation processes, a wide variety of particle structures are produced. Considering coagulation kinetics of fractal-like particles, we assume that the cluster fractal dimension $D_f(k)$ depends on number of atoms k in a cluster. This allows us to describe the whole spectrum of cluster sizes starting from dimers. We assume that small clusters grow spherical up to the radius $R_0 = r_{Cu}\sqrt[3]{k_0}$, where k_0 is the number of atoms (see Table I). Larger clusters grow in the form of fractal-like aggregates. As the clusters drift with the Ar flow to the aperture, a fraction of small spherical clusters migrate to wall. The remaining clusters collide with each other to form fractal-like aggregates. In our model, we define the collision radius of clusters R_c as

$$R_c(k) = R_0\left(\frac{k}{k_0}\right)^{\frac{1}{D_f(k)}}. \tag{22}$$

To test the model, for the fractal dimension $D_f(k)$, we choose a simple decreasing function of cluster size k (Fig. 2),

$$D_f(k) = \begin{cases} 3 \quad \text{at} \quad k \le k_0, \\ D_f^{\infty} + (3 - D_f^{\infty})\left[1 + \left(\dfrac{k - k_0}{10k_0}\right)^2\right]^{-1} \quad \text{at} \quad k > k_0, \end{cases} \tag{23}$$

where $D_f^{\infty} = \lim_{k\to\infty} D_f(k)$ is the fractal dimension of the largest clusters in the system.

The size dependence of the collision radius is shown in Fig. 2. The collision radius of a small spherical cluster ($k \le k_0$) coincides with its radius. The collision radius of fractal-like cluster ($k > k_0$) is larger than the radius of the spherical cluster with the same number of atoms. Instead of Eq. (18), we will use the modified coagulation kernel that is appropriate both for small spherical clusters and large fractal-like ones,

$$w_{ij} = \eta_{ij}\left(R_c(i) + R_c(j)\right)^2\sqrt{\frac{8\pi k_B T}{m_{Cu}}\left(\frac{1}{i} + \frac{1}{j}\right)}. \tag{24}$$

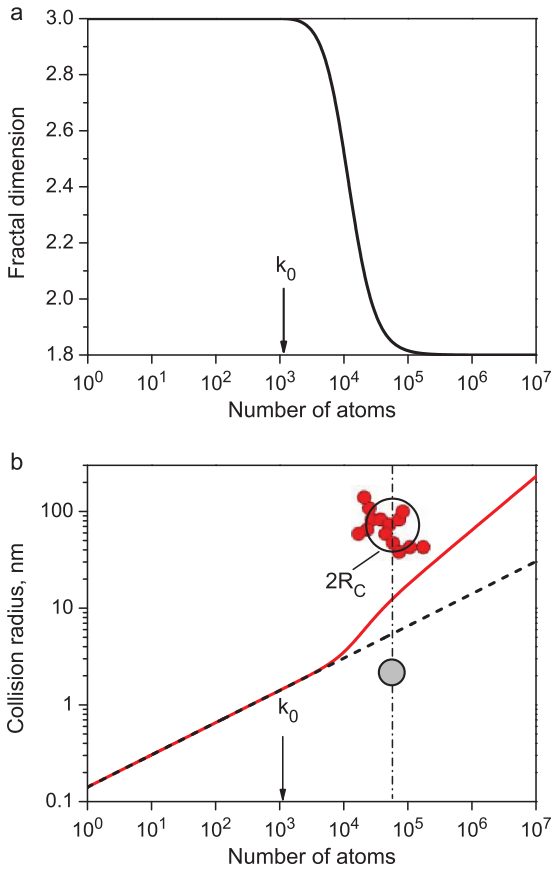

FIG. 2. The size dependence of the cluster fractal dimension (a) and collision radius (b). The solid line refers to fractal-like cluster. The dashed line shows the radius of the spherical cluster with the same number of atoms.

B. Cluster diffusion coefficient

In the following, we will use the cluster diffusion coefficient in the form of Eq. (7), assuming that the diffusion of agglomerate is equal to the diffusion of a sphere with equivalent volume. For small clusters, their diffusion transport in the buffer gas has similarities to molecular transport. As the size of the nanoparticle increases, momentum exchange with the gas atoms and nanoparticle inertia are different, extending into the regime where corrections to the gas model can be used.[20] Transport properties of fractal-like particles in gases differ to that of spheres, i.e., nanoparticle morphology has to be taken into account in addition to their size.[19,20] The diffusion coefficient of fractal-like clusters can be roughly estimated by assuming that Ar atoms collide with the sphere having the effective collision radius of fractal-like clusters,

$$D_k^{Fractal} = \frac{1}{3}\sqrt{\frac{2}{\pi}}\sqrt{\frac{1}{m_{Ar}} + \frac{1}{k\,m_{Cu}}}\,\frac{(k_B T)^{3/2}}{P_{Ar}\pi\left(r_{Ar} + R_c(k)\right)^2}. \tag{25}$$

In Fig. 3, the solid line shows the diffusion coefficient given by Eq. (7). This equation overestimates the mobility of fractal-like clusters. The dash-dotted line corresponds to Eq. (25). This diffusion coefficient strongly underestimates diffusion mobility of large fractal-like clusters with $k \gg k_0$. The reason is that agglomerates with fractal dimensions smaller than 3 have an open structure which is transparent to atoms

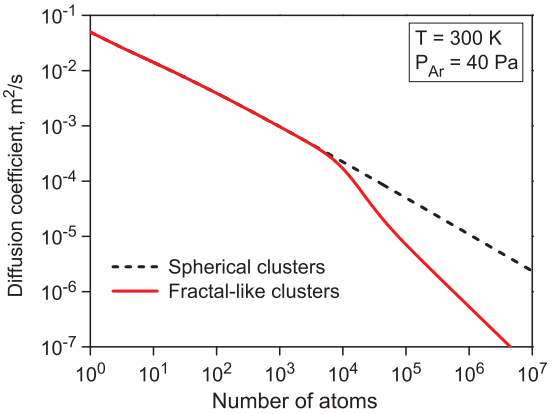

FIG. 3. Diffusion coefficients of spherical clusters (dashed line, Eq. (7)) and fractal-like clusters (solid line, Eq. (25)).

from the surrounding Ar gas. In other words, when the size disparity between colliding particles (Ar atom versus cluster) is large the sum of collision radii overestimates the number of collisions.[21]

We have made simulations of cluster evolution with both coefficients, Eqs. (7) and (25). The results are about the same. The difference between distribution functions is in a few percent range. The reason is that for large clusters diffusion migration to macroscopic distances (to walls) takes time R^2/D_k which is greater than the residence time of clusters in the aggregation tube even when we use the diffusion coefficient of spherical clusters, $R^2/D_k > 10s > \tau_{max}$ at $k > 10^4$. The main mechanism that controls the evolution of size distribution of large clusters is the coagulation of colliding clusters.

C. Numerical method

Because of nonlinearity and complexity, the set of equations for PSD [Eqs. (14)–(17)] can be solved only numerically. However, this problem is impossible to solve directly, even numerically, since the number of coupled equations amounts to the number of atoms in the largest cluster present in the system, i.e., requirements to computer resources increase enormously with the cluster size. This difficulty is common in the description of evolution of cluster populations. The general solution strategy for the set of equations for PSD is to reduce it to a numerical scheme with a controlled number of equations. Existing numerical methods are reviewed in Refs. 22–25.

In our study, to decrease drastically the number of equations, we propose a new approach that is rather simple and straightforward methodologically as compared to methods described in the literature. First, we notice that the set of ordinary differential equations (ODEs) given by Eq. (15) is the discretized version of the integro-differential equation for the continuous cluster sizes variable z,

$$\frac{\partial C(z)}{\partial \tau} = -\nu\mu(D(z))C(z) + \int_0^{z/2} W(z-y,y)C(z-y)C(y)dy - C(z)\int_0^{\infty} W(z,y)C(y)dy. \quad (26)$$

Indeed, Eq. (15) is recovered by replacing integration with the trapezoidal summation on the discrete size mesh $z_k = k$, $k = 0, 1, 2, \ldots$ with additional constrains $C(0) = 0$ and $C(1) = C_1$. The size variable and coagulation kernel are changed correspondingly as

$$k \Longleftrightarrow z_k, \quad C_k \Longleftrightarrow C(z_k), \quad w_{ij} \Longleftrightarrow W(z_i, z_j).$$

Therefore, instead of Eq. (15), we will solve the equivalent integro-differential equation (26). In the next step, we transform this equation into a new set of ODE for discrete cluster sizes on a coarse mesh with the increasing mesh spacing. For our purposes, the following relations for mesh points z_k and mesh spacings Δz_k are used:[26]

$$\begin{aligned} &z_1 = 1, \\ &z_k = z_{k-1} + \Delta z_k \quad 2 \le k \le K, \\ &\Delta z_k = \begin{cases} 1 & \text{at } 2 \le k \le N, \\ \Delta x_{k-1}\exp(\varepsilon) & \text{at } N < k \le K, \end{cases} \end{aligned} \quad (27)$$

where K is sufficiently large so that the boundary condition $C(z_K) = 0$ is fulfilled to a good accuracy. The variation of mesh spacing is controlled by the parameter ε that should be positive and small, $0 < \varepsilon \ll 1$. The spacing between mesh points increases exponentially with point number $k > N$, $\Delta z_k = \exp[\varepsilon(k-N)]$. Therefore, due to coarse-graining of the numerical mesh, the number of equations can be reduced substantially (typically by a factor of 10^3–10^4) as compared to the initial set of discrete equations. The number of equations is controlled by the parameters ε.

For the integration, we use the trapezoidal summation rule for unequally spaced abscissae. The integral in the third term of the right-hand-side of Eq. (26) is given by

$$\int_0^{\infty} W(z_k, y)C(y)dy = \sum_{i=1}^{K} W(z_k, z_i)C(z_i)\Delta u_i, \quad (28)$$

where $\Delta u_i = 0.5(\Delta z_i + \Delta z_{i+1})$.

For the cluster densities $C_k = C(z_k)$ in the equidistant mesh points $z_k = k \le N$, the convolution integral given by the second term in the right-hand-side of Eq. (26) is evaluated using the original equation (15) for discrete cluster sizes. For cluster density in mesh points $z_k > N$, the convolution integral is estimated as follows:

$$\int_0^{z_k/2} W(z_k - y, y)C(z_k - y)C(y)dy = \sum_{i=1}^{k_2-1} W(z_k - z_i, z_i)C(z_k - z_i)C(z_i)\Delta u_i + R_k, \quad (29)$$

where k_2 is the index of the mesh point that satisfies the condition $z_{k_2} \le z_k/2 < z_{k_2+1}$.

The remainder term R_k is given by

$$R_k = \frac{1}{2}F_{k_2}\Delta z_{k_2} + \left[F_{k_2} + \frac{1}{2}\frac{F_{k_2+1} - F_{k_2}}{\Delta z_{k_2+1}}\left(\frac{z_k}{2} - z_{k_2}\right)\right]\left(\frac{z_k}{2} - z_{k_2}\right), \quad (30)$$

where $F_m = W(z_k - z_m, z_m)C(z_k - z_m)C(z_m)$, $m = k_2, k_2 + 1$.

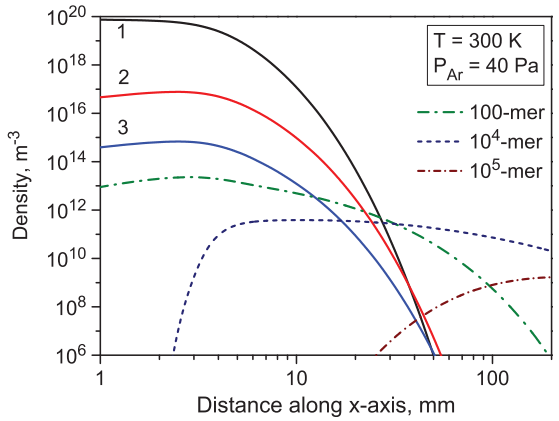

FIG. 4. Dependence of cluster densities along the aggregation tube. The coagulation kernel equation (18) for spherical clusters was used in the calculations. Solid lines labeled with 1, 2, and 3 refer to monomers, dimers, and trimers, respectively.

To evaluate $W(z_k - z_i, z_i)$ and $C(z_k - z_i)$ in Eqs. (29) and (30), the linear interpolation between two neighboring mesh points is used.

The initial value problem for the set of ODE obtained by the procedure described above can be solved by a standard numerical package for stiff ODE sets. Stiffness is the generic feature of this type of evolution equations; it is related to the fact that densities of monomers and small clusters change very fast as compared to slow changes in densities of large clusters. We use the RADAU code that has been developed for stiff and differential-algebraic problems.[27] This code is based on the implicit Runge-Kutta method of variable order with an adaptive time-step control.

Direct comparison of the calculated PSDs and their moments to available analytical solutions of coagulation equations with simple kernels, $w_{ij} = const$, $w_{ij} = i + j$, and $w_{ij} = ij$, confirmed a very good performance of the numerical method described above. The detailed description of the numerical method will be presented elsewhere.

III. RESULTS OF MODELING

The coagulation equations (14)–(17) were solved by the method described above using parameters listed in Table I. The initial density of Cu atomic vapor was found from the diffusion equation without coagulation; $C^0_{axis} = C|_{r=0,x=0} = 7.83 \times 10^{19}\,\mathrm{m}^{-3}$. The initial set of equations given by Eqs. (14) and (15) consists of about 4.5×10^7 equations, which corresponds to the maximum radius of the spherical clusters of 50 nm. Using mesh parameters $N = 100$ and $\varepsilon = 0.02$, this set is transformed into a set of 785 equations on the coarse mesh described by Eq. (27). On a standard PC with CPU Intel 2.4 GHz, the solution time amounts to about 1.5 min.

First, we present modeling results obtained with the coagulation kernel equation (18) for spherical clusters. Figure 4 shows the dependences of cluster densities as a function of position in the aggregation tube. It is seen that the densities of monomers and small-sized clusters decrease very fast because of diffusion to walls. Larger clusters appear after some delay, as a result of collisions and aggregations while drifting to the aperture. When atoms begin to condense, the cluster growth first proceeds by successive addition of monomers and small clusters (dimers, trimers, etc.), and when the supply of these decreases, coalescence of larger clusters increasingly contributes to PSD evolution.

Figure 5 shows the nanocluster size distributions at various positions in the aggregation tube. The size distribution $F(r)$ is defined by relations

$$F(r_k) = \frac{3}{r_1} k^{2/3} C_k, \quad \sum_{k=2}^{\infty} C_k = \int_{r_2}^{\infty} F(r)dr. \qquad (31)$$

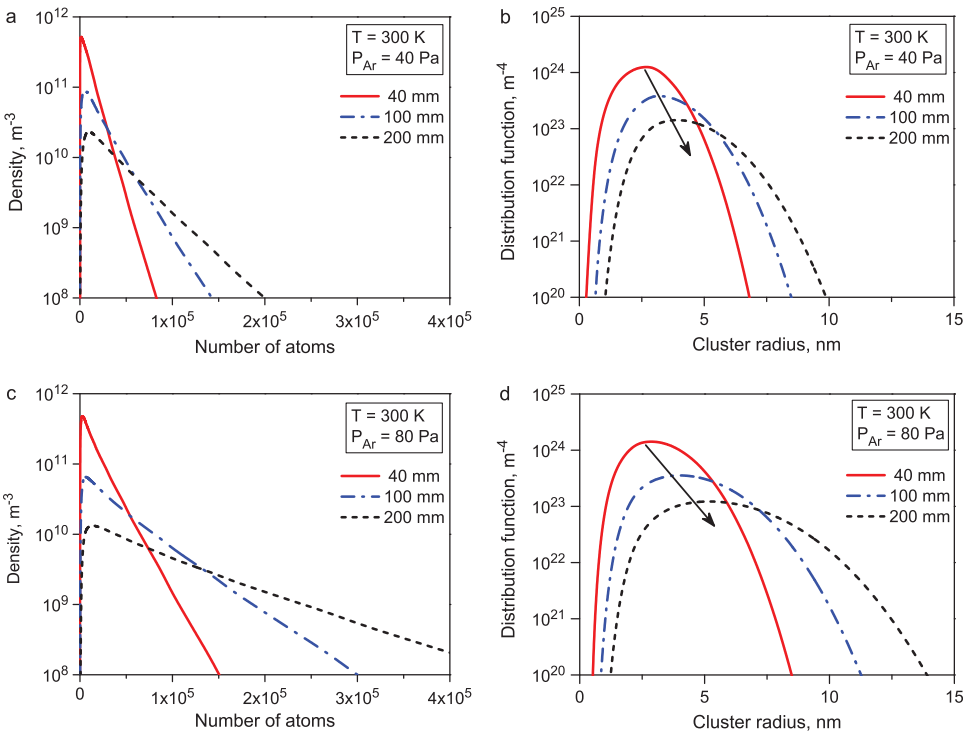

FIG. 5. Cluster size distributions in terms of number of atoms in clusters C_k (left) and cluster radii $F(r)$ (right) at various positions in the aggregation tube. The top and bottom rows of figures were calculated at Ar pressures 40 Pa and 80 Pa, respectively. It was assumed that the Ar pressure is proportional to the rate of Ar flow Q_{Ar}. The coagulation kernel equation (18) for spherical clusters was used in the calculations.

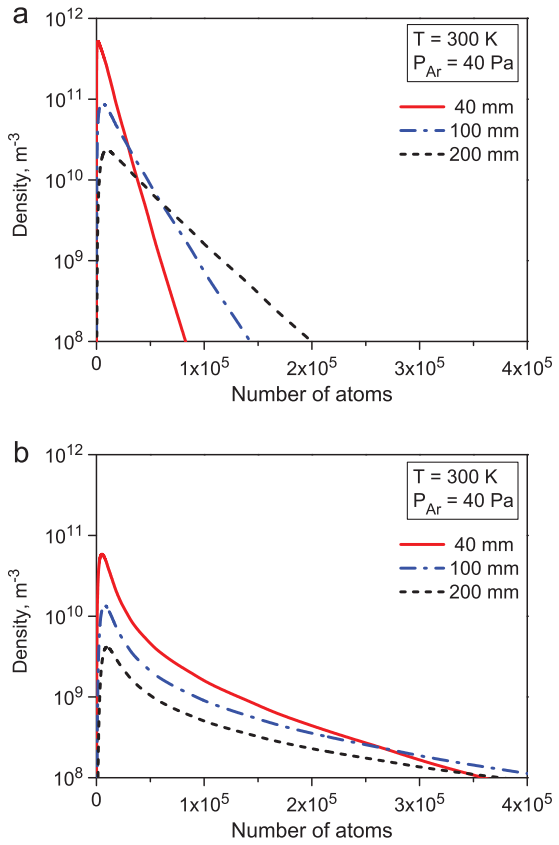

FIG. 6. The nanocluster size distribution calculated with the "spherical" coagulation kernel equation (18) (a) and with the "fractal" coagulation kernel equation (22) (b). Other parameters are the same for both figures.

The arrow in the right figures indicates a shift of the distribution maximum to larger sizes. Note that increase in Ar pressure enhances the coagulation, i.e., the distribution becomes broader. The reason is that the cluster diffusivity decreases (see Eq. (7)), hence the cluster loss to wall reduces.

To demonstrate the dependence of cluster deposition onto the walls on cluster size, we have performed an experiment. A stripe of stainless steel was placed inside the aggregation tube along the cylindrical wall. After several minutes, the sputtered copper deposited to the stripe. The part of stripe which was close to the magnetron exhibited a typical red color of polished copper indicating that copper atoms and small clusters deposited to this part. The mid-portion of the stripe was black because of cluster deposition. The part of stripe near the aperture did not change its color, i.e., a very small number of clusters deposited here. We interpret it as a consequence of slow diffusion of large clusters.

The influence of cluster morphology on PSD evolution was modeled with coagulation kernel equation (24) (Fig. 6). The distribution of fractal-like particles is very broad as compared to the distribution of spherical clusters. The mean

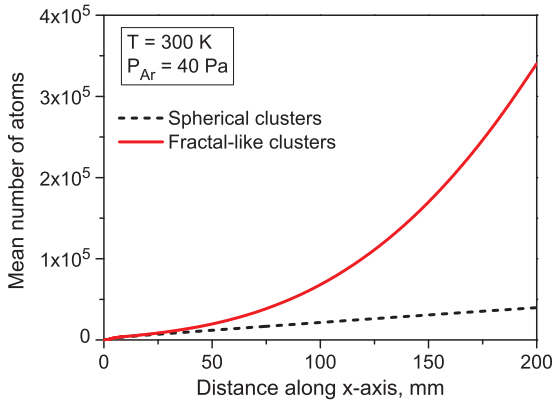

FIG. 7. Mean number of atoms in spherical and fractal-like clusters. The dashed line corresponds to modeling with the "spherical" coagulation kernel equation (18). The solid line is modeled with the "fractal" coagulation kernel Eq. (22).

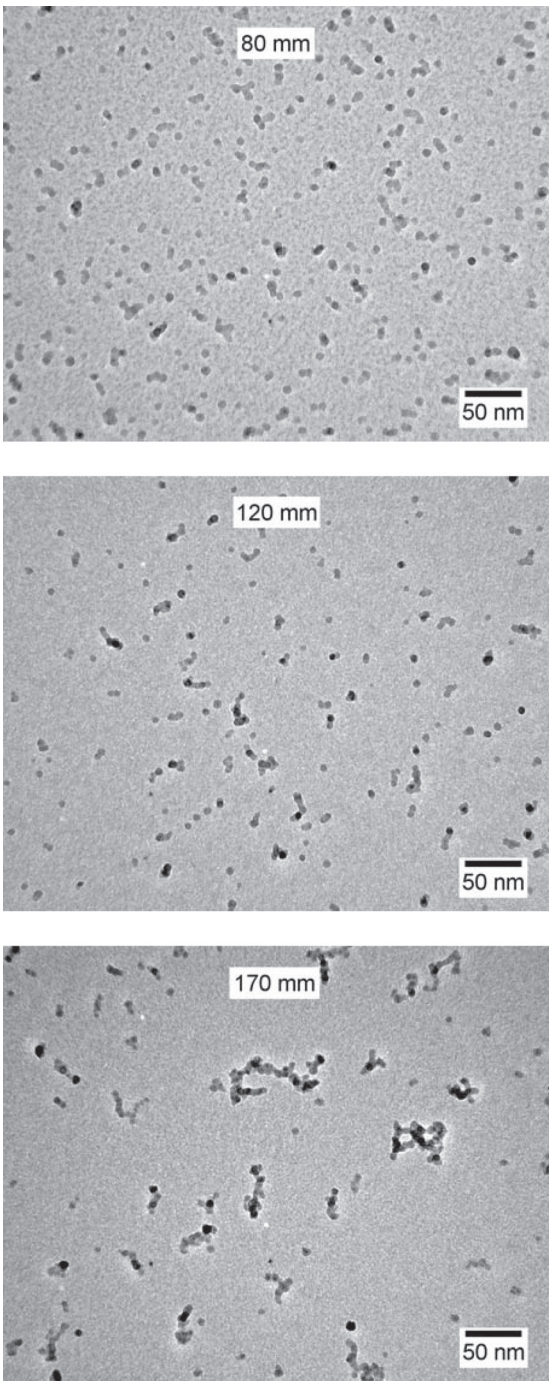

FIG. 8. TEM pictures of Cu clusters collected inside the aggregation tube close to its axis in 15 s deposition time.

number of atoms in fractal-like particles is substantially greater than in spherical particles grown under the same conditions, calculated with the "spherical" coagulation kernel equation (18) (Fig. 7).

IV. COMPARISION WITH EXPERIMENTS

To collect formed clusters, TEM grids were placed inside the aggregation tube, close to its axis at distances 80, 120, and 170 mm from the Cu target. Figure 8 shows the TEM images of Cu clusters collected during deposition time of 15 s. At the distance of 80 mm from the Cu target, the density of deposited clusters is high and the contrast from individual clusters overlap. However, it appears that the shape of clusters is compact and close to spherical. Near the end of aggregation chamber (170 mm from the Cu target), the clusters are undoubtedly dendrite-like with maximum sizes in the range of 50 nm.

The area density of deposited cluster N_S were recalculated into the total volume density of cluster $N_V = \sum_{k>1} C_k$ using the relation

$$N_S = N_V v t. \tag{32}$$

Figure 9 compares the experimental data with the model calculations. To obtain a good agreement, two parameters, k_0 and D_f^{∞}, were adjusted. It is noteworthy that $D_f^{\infty} = 1.8$ is close to the value observed during diffusion limited cluster aggregation.[7,18,19]

To find the cluster PSD $F_V^{\exp}(n)$, the surface distribution $F_S(A)$ over the cluster projected area A was measured. Then we used the formula[18] that relates the cluster projected area A and the number of atoms n in a cluster

$$n = k_0 k_a \left(\frac{A}{\pi r_{Cu}^2 k_0^{2/3}} \right)^{\alpha_a}, \tag{33}$$

where k_a and α_a are the fitting parameters (notation of Ref. 18). The cluster size distribution $F_V^{\exp}(n)$ is given by

$$F_V^{\exp}(n) = \frac{F_S(A)}{vt} \frac{dA}{dn}. \tag{34}$$

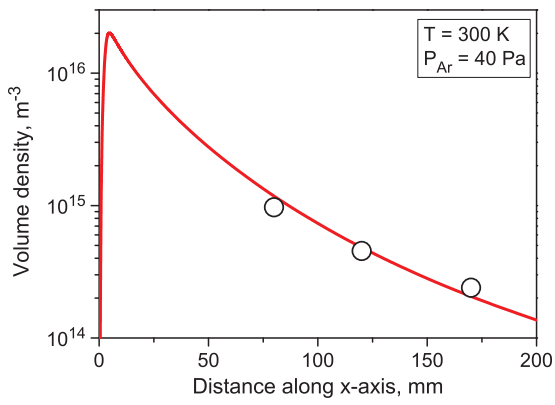

FIG. 9. The volume density of fractal-like Cu nanoparticles as a function of distance from the Cu target. Experimental data are shown by open symbols.

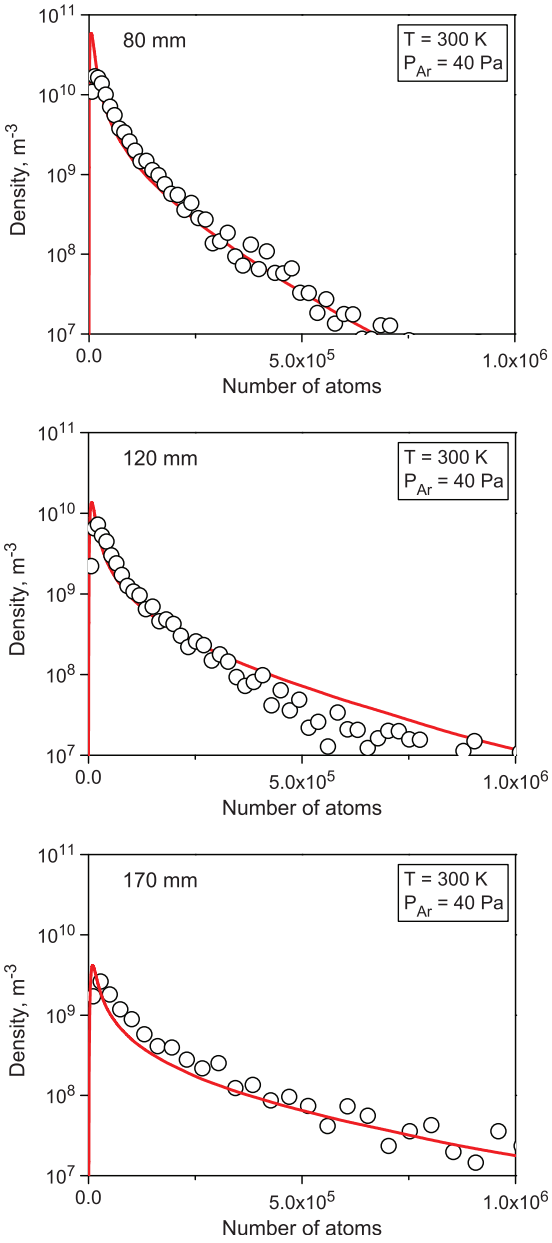

FIG. 10. The size distribution of nanoclusters at distances 80, 120, and 170 mm from the Cu target. Symbols correspond to experimental distributions $F_V^{\exp}(n)$ reconstructed from surface distributions $F_S(A)$ using Eqs. (33) and (34). Fitting parameters $k_a = 3$ and $\alpha_a = 1.4$ (see Eq. (33)). The solid line shows results of modeling.

Comparison between experimental and model distributions is presented in Fig. 10. For appropriately chosen parameters, a good agreement can be achieved between the experimental data and predictions of the proposed method.

V. CONCLUSIONS

(1) A new model of cluster formation from a supersaturated atomic vapor in an inert gas flow has been formulated. We show that the following concurrent processes govern the evolution of nanocluster size distribution:
- convective diffusion of clusters,
- cluster loss to walls of an aggregation chamber,
- the Smoluchowski coagulation,

- formation of fractal-like aggregates.

(2) An efficient and adequate numerical technique for solving population balance equation involving aggregation has been developed. Other particulate processes such as particle fragmentation, growth, and nucleation can be easily included in the numerical technique proposed.

(3) The model predictions consist well with the experimental data on the particle size distribution of Cu nanoparticle formed in NC200-UHV nanocluster source. In this installation, the cluster size distribution can be controlled by adjusting the power supplied to the magnetron (i.e., the sputtering rate of precursor), the exit aperture size, the type and flow rate of inert gases, temperature and pressure in the aggregation tube, and distance between the atomic vapor source and the aperture. These control parameters can be tuned in the model making it a useful aid for future experiments so as to control the width and character of the size-distribution.

ACKNOWLEDGMENTS

The Netherlands Organization for Scientific Research NWO is acknowledged for awarding a visitor's grant to one of the authors (A.A.T.).

APPENDIX A: SOLUTION TO DIFFUSION EQUATION WITHOUT COAGULATION

Consider the steady-state convective diffusion of Cu monomers in the approximation of plug flow of gas in the aggregation chamber,

$$v\frac{\partial C}{\partial x} = D\Delta C. \tag{A1}$$

Here, we are going to find a recipe how to reduce 3D diffusion problem to a 1D diffusion problem, so for a moment we neglect monomer absorption by Cu clusters. Equation (A1) satisfies boundary conditions of Eqs. (10)–(12). For simplicity, we do not take into account the influence of aperture on diffusion. According to Ref. 28, the solution of Eq. (A1) is given by

$$C(r,x) = \frac{4}{R^2 v}\sum_{i=1}^{\infty}\frac{J_0(\beta_i r/R)}{J_1(\beta_i)^2}G_i(x)\int_0^R rq(r)J_0(\beta_i r/R)dr, \tag{A2}$$

where $J_n(..)$ is the Bessel function of the order n of the first kind; $\beta_i = 2.2048, 5.5201, 8.6537,\ldots$ are the positive roots of $J_0(\beta_i) = 0$. The longitudinal dependence of the density is described by functions

$$G_i(x) = \exp\left(\frac{v}{2D}x\right)\frac{\sinh[\gamma_i(L-x)]}{2Dv^{-1}\gamma_i\cosh(\gamma_i L)+\sinh(\gamma_i L)}, \tag{A3}$$

where $\gamma_i = \frac{v}{2D}\sqrt{1+\left(\frac{2D}{vR}\right)^2\beta_i^2}$.

For the parabolic source of Cu atoms sputtered from the target, Eq. (12), the solution is given by

$$C(r,x) = \frac{32\,Q_{Cu}}{\pi R^2 v}\sum_{i=1}^{\infty}\frac{J_0(\beta_i r/R)}{\beta_i^3 J_1(\beta_i)}G_i(x). \tag{A4}$$

For a long cylinder $L > R$, the function $G_i(x)$ transforms into a simple expression describing the exponential decay of density along the x-axis

$$G_i(x) = \left(\sqrt{1+\left(\frac{2D}{vR}\right)^2\beta_i^2}+1\right)^{-1} \times \exp\left[-\frac{v}{2D}\left(\sqrt{1+\left(\frac{2D}{vR}\right)^2\beta_i^2}-1\right)x\right]. \tag{A5}$$

Taking into account only the first term of the sum in Eq. (A4), we approximate the density change along the aggregation tube axis by the expression

$$C_{axis}(x) = C^0_{axis}\exp(-\mu x), \tag{A6}$$

where

$$\mu = \frac{v}{2D}\left(\sqrt{1+\left(\frac{2D}{vR}\right)^2\beta_1^2}-1\right), \tag{A7}$$

and C^0_{axis} is the density at $x = 0$ and $r = 0$ found from Eqs. (A4) and (A5),

$$C^0_{axis} = \frac{32Q_{Cu}}{\pi R^2 v}\sum_{i=1}^{\infty}\frac{1}{\beta_i^3 J_1(\beta_i)}\left(\sqrt{1+\left(\frac{2D}{vR}\right)^2\beta_i^2}+1\right)^{-1}. \tag{A8}$$

The approximate solution given by Eq. (A6) satisfies the equation

$$\frac{dC}{dx} = -\mu C. \tag{A9}$$

Comparison of this equation with Eq. (A1) shows that the diffusion operator can be replaced with multiplication by a constant, i.e.,

$$D\Delta C \Rightarrow -v\mu(D)\,C. \tag{A10}$$

We use a relation (A10) for clusters of all size classes. Figure 11 compares the exact and approximate solutions to the convective-diffusion equation (A1). It is seen that at $D = D_1$ approximate solutions well describe the dependence of monomer density on distance. According to estimations, for monomers and small cluster, the Peclet numbers $\mathrm{Pe_k} = vR/D_k$ are small ($\mathrm{Pe_1} = 0.1$ and $\mathrm{Pe_{70}} = 1.1$), i.e., the diffusion transport dominates the convective one; and the length scale for density change is R/β_1. This means that due to high diffusion mobility monomers and small cluster are deposited to walls.

For large clusters, the convective transport dominates, $\mathrm{Pe_k} \gg 1$; and some of these clusters can escape the aggregation tube through the aperture to deposit on a sample

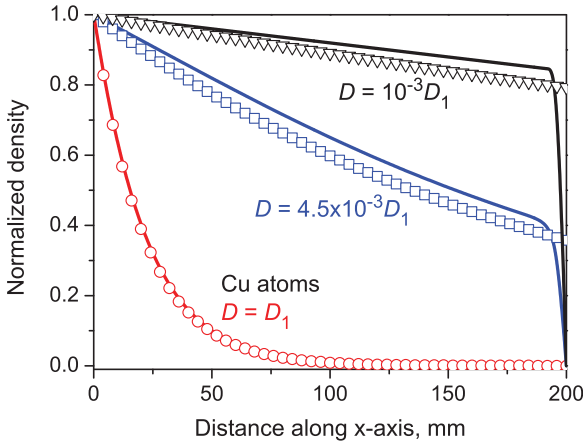

FIG. 11. Comparison between the exact solutions (Eq. (A4) at $r = 0$, solid curves) and the approximate solutions (Eq. (A6), symbols) to the convective diffusion equation (A1) at several values of the diffusion coefficient. The diffusion coefficient of Cu monomer $D_1 = 0.05$ m^2/s. The diffusion coefficient $D = 10^{-3}D_1$ corresponds to a cluster size $k = 10^5$ atoms (spherical cluster of diameter 12 nm).

substrate. Figure 11 shows that replacement (A10) works well for large clusters except close proximity of $x = L$, where we set the boundary condition $C|_{x=L} = 0$.

APPENDIX B: FORMATION RATE OF STABLE CU DIMER

The density of metastable Cu-dimers C_2^* change with time according to

$$\frac{dC_2^*}{dt} = \frac{1}{2}\alpha^* C_1^2 - \alpha_{Ar} C_{Ar} C_2^* - \frac{C_2^*}{\tau_d}. \tag{B1}$$

In this equation, only the most probable processes are taken into account (collisions with monomers and other clusters are rare). Stable dimers form in collisions with Ar atoms

$$\frac{dC_2}{dt} = \alpha_{Ar} C_{Ar} C_2^* + (.....), \tag{B2}$$

where (.....) denotes slow processes (cluster loss to coagulation and diffusion). To derive the rate coefficient α^* and α_{Ar} we follow closely Refs. 5 and 17. It was assumed that the Cu atoms interact via the Lennard-Jones potential,[5]

$$V(r) = 4\varepsilon\left[\left(\frac{\sigma}{r}\right)^{12} - \left(\frac{\sigma}{r}\right)^{6}\right] \tag{B3}$$

with the parameters $\varepsilon = 2.03$ eV and $\sigma = 0.198$ nm. The cross-section for orbiting complex formation is given by

$$\Sigma_{orb} = 3\pi\sigma^2(\varepsilon/E_{rel})^{1/3}, \tag{B4}$$

where E_{rel} is the relative kinetic energy of two Cu atoms. Therefore, the rate constant for the metastable complex formation is written as

$$\alpha^* = 4\Sigma_{orb}\sqrt{\frac{k_B T}{\pi m_{Cu}}}. \tag{B5}$$

The rate constant α_{Ar} for collision between an Ar atom and the metastable complex is given by

$$\alpha_{Ar} = \frac{2}{3}\Sigma_{orb}\sqrt{\frac{8k_B T}{\pi m_{Cu}}\left(\frac{m_{Cu}}{m_{Ar}} + \frac{1}{2}\right)}. \tag{B6}$$

The lifetime τ of the metastable orbiting complex[5]

$$\tau_d = 1.5\sigma\sqrt{\frac{m_{Cu}}{2\varepsilon}}\left(\frac{\varepsilon}{E_{rel}}\right)^{2/3}. \tag{B7}$$

It is reasonable to assume that formation and decay of metastable orbiting complexes are fast processes maintaining a quasi steady state,

$$\frac{1}{2}\alpha^* C_1^2 - \alpha_{Ar} C_{Ar} C_2^* - \frac{C_2^*}{\tau_d} = 0. \tag{B8}$$

From Eqs. (B2) and (B8), we find the rate of stable dimer formation

$$\frac{dC_2}{dt} = \frac{1}{2}\alpha_{dimer} C_1^2 + (.....), \tag{B9}$$

where α_{dimer} is the rate constant,

$$\alpha_{dimer} = \frac{\alpha^* \alpha_{Ar} C_{Ar} \tau_d}{1 + \alpha_{Ar} C_{Ar} \tau_d}. \tag{B10}$$

In our case, $\alpha_{Ar} C_{Ar} \tau \sim 10^{-6}$. Therefore, the sticking coefficient of dimer formation is given by

$$\eta_{11} = \alpha_{dimer}\left(16 r_{Cu}^2\sqrt{\frac{\pi k_B T}{m_{Cu}}}\right)^{-1} = \frac{9\sqrt{\pi}\sigma^5}{2r_{Cu}^2}\sqrt{\frac{1}{2} + \frac{m_{Cu}}{m_{Ar}}}\left(\frac{k_B T}{E_{Rel}}\right)^{4/3}\left(\frac{\varepsilon}{k_B T}\right)^{5/6} C_{Ar}. \tag{B11}$$

At $T = 300$ K, $P_{Ar} = 40$ Pa (Table I) and $E_{rel} = 3k_B T$, the sticking coefficient is estimated as

$$\eta_{11} = 1.8 \times 10^3 C_{Ar} r_{Ar}^3 \approx 1.55 \times 10^{-5}. \tag{B12}$$

[1] *Metal Nanoclusters in Catalysis and Materials Science: The Issue of Size Control*, edited by B. Corain, G. Schmid, and N. Toshim (Elsevier B.V., 2008).
[2] J. A. Alonso, *Structure and Properties of Atomic Nanoclusters* (Imperial College, 2005).
[3] *Nanomaterials: Design and Simulation*, Theoretical and Computational Chemistry Vol. **18**, edited by P. B. Balbuena and J. M. Seminario (Elsevier B.V., 2007).
[4] See *UnderstandingNano.com*, http://www.understandingnano.com for a list and description of nanotechnology applications.
[5] B. Briehl and H. M. Urbassek, J. Vac. Sci. Technol. A **17**, 256 (1999).
[6] H. Mizuseki, Y. Jin, Y. Kawazoe, and L. T. Wille, Appl. Phys. A **73**, 731 (2001).
[7] S. K. Friedlander, *Smoke, Dust and Haze: Fundamentals of Aerosol Dynamics*, 2nd ed. (Oxford University Press, 2000).
[8] P. Roth, Proc. Combust. Inst. **31**, 1773 (2007).
[9] A. Camenzind, W. R. Caseri, and S. E. Pratsinis, Nanotoday **5**, 48 (2010).
[10] P. Meakin, *Fractals, Scaling and Growth Far from Equilibrium* (Cambridge University Press, Cambridge, 1998).

[11]T. Matsoukas and S. K. Friedlander, J. Colloid Interface Sci. **146**, 495 (1991).
[12]M. K. Wu and S. K. Friedlander, J. Aerosol Sci. **24**, 273 (1993).
[13]T. I. Gombosi, *Gaskinetic Theory* (Cambridge University Press, 1994).
[14]R. B. Bird, W. E. Stewart, and E. N. Lightfoot, *Transport Phenomena* (Wiley, New York, 1960).
[15]M. V. Smoluchowsky, Z. Phys. Chem. **92**, 129 (1917).
[16]L. Boltzmann, *Vorlesung Uber Gastheorie II* (J. A. Barth, Leipzig, 1989).
[17]D. L. Bunker, J. Chem. Phys. **32**, 1001 (1960).
[18]A. M. Brasil, T. L. Farias, and M. G. Carvalho, J. Aerosol Sci. **30**, 1379 (1999).
[19]C. M. Sorensen, Aerosol Sci. Technol. **45**, 765 (2011).
[20]L. Mädler and S. K. Friedlander, Aerosol Air Quality Res. **7**, 304 (2007).
[21]M. Zurita-Gotor and D. E. Rosner, J. Colloid Interface Sci. **255**, 10 (2002).
[22]A. I. Roussosa, A. H. Alexopoulos, and C. Kiparissides, Chem. Eng. Sci. **61**, 124 (2006).
[23]J. Kumar, M. Peglow, G. Warnecke, and S. Heinrich, Powder Technol. **182**, 81 (2008).
[24]V. Saliakas, C. Kotoulas, D. Meimaroglou, and C. Kiparissides, Can. J. Chem. Eng. **86**, 924 (2008).
[25]J. Kumar, "Numerical approximations of population balance equations in particulate systems," PhD thesis, Otto-von-Guericke-University Magdeburg, Germany, 2006.
[26]A. A. Turkin and A. S. Bakai, J. Nucl. Mater. **358**, 10 (2006).
[27]E. Hairer and G. Wanner, *Solving Ordinary Differential Equations II. Stiff and Differential-Algebraic Problems*, Springer Series in Computational Mathematics Vol. 14 (Springer-Verlag, 1996).
[28]H. S. Carslaw and J. C. Jaeger, *Conduction of Heat in Solids*, 2nd ed. (Clarendon, Oxford, 1959).